

Measurement of Σ^+ transverse polarization in e^+e^- collisions at $\sqrt{s} = 3.68 - 3.71$ GeV



The BESIII Collaboration

E-mail: besiii-publications@ihep.ac.cn

ABSTRACT: Using e^+e^- collision data collected with the BESIII detector at seven energy points ranging from 3.68 to 3.71 GeV and corresponding to an integrated luminosity of 652.1 pb^{-1} , we present an energy-dependent measurement of the transverse polarization, relative phase and modulus ratio of the electromagnetic form factors of the Σ^+ hyperon in the $e^+e^- \rightarrow \Sigma^+\bar{\Sigma}^-$ reaction. These results are helpful to understand the production mechanism of the $\Sigma^+\bar{\Sigma}^-$ pairs.

Contents

1	Introduction	1
2	BESIII detector and Monte Carlo simulation	3
3	Event selection	3
4	Σ^+ polarization	4
5	Systematic uncertainty	8
5.1	$\Sigma^+(\bar{\Sigma}^-)$ reconstruction	10
5.2	Mass window	10
5.3	Background	10
5.4	Fit method	10
5.5	Decay parameter	11
5.6	Total systematic uncertainty	11
6	Summary	11

1 Introduction

As early as 1960, the significance of baryon structure was widely acknowledged [1]. However, at present, understanding the structure of baryons remains a great challenge. Apart from protons and neutrons, knowledge has been relatively scarce. The proton, being a stable particle, allows for the determination of the space-like electromagnetic form factors (EMFFs) via elastic electron-proton scattering [2]. More recently, e^+e^- collisions, resulting in the production of baryon pairs, provide an ideal experimental framework to study baryon structure. This is because the e^+e^- process offers access to the time-like EMFFs via virtual photon production, thereby facilitating the quantitative assessment of baryonic electromagnetic structure. Experimentally accessible time-like EMFFs are intimately connected with more intuitive space-like quantities, such as charge and magnetization densities, through the dispersion relation [3, 4]. Baryon pairs with a spin of 1/2 produced by the e^+e^- process via a virtual photon are elegantly described by two distinct EMFFs: the electric form factor G_E and magnetic form factor G_M [5, 6]. These form factors are functions of the square of the four-momentum transfer, denoted as q^2 . In the time-like region, where $q^2 > 0$, the EMFFs exhibit non-zero imaginary components. Consequently, when G_E and G_M are different, they give rise to a relative phase denoted as $\Delta\Phi = \Phi_E - \Phi_M$, where Φ_E and Φ_M are the phases of G_E and G_M , respectively.

In accordance with the Phragmén-Lindelöf theorem [7], as $q^2 \rightarrow \infty$, the asymptotic behavior of the time-like EMFFs can be obtained from their corresponding space-like counterparts. In the space-like region, the EMFFs are assumed to be real. Consequently, as $q^2 \rightarrow \infty$, the time-like EMFFs must also be real, and the relative phase of the EMFFs should approach an integer multiple of π . In the case where q^2 does not approach the limit, the phase can be any value other than zero, which causes the final state to be polarized, even if the initial state is unpolarized [8]. This allows the determination of the EMFFs, as the polarization and cross-section are functions of form factors themselves [9–11]. Recent results from BESIII [12], BaBar [6] and Belle [13], focusing solely on measuring the effective form factor, have reported consistent results. Additionally, the CLEO collaboration has made significant progress in determining the cross sections and the EMFFs of various baryon pairs (p , Λ , Σ^0 , Σ^+ , Ξ^0 , Ξ^- , and Ω^-) [14, 15]. Their conclusions regarding EMFFs and di-quark correlations [16, 17] rely on the assumption that one-photon exchange dominates the production process and that charmonia contributions are negligible. Furthermore, the BESIII collaboration has measured the cross sections for several baryon pairs (Λ , Σ^0 , Ξ^- , Σ^\pm , and Ξ^0) near the production threshold [12, 18–22] and above open charm threshold [24–28]. However, experimental measurements of the relative phase between G_E and G_M are still relatively scarce.

For spin 1/2 baryon pairs produced by the e^+e^- process via vector charmonia, where the above statements concerning EMFFs also apply, the formalism is described in ref. [9]. In these cases, the amplitudes include the EM-*psionic* form factors, G_E^Ψ and G_M^Ψ [29, 30]. While the EM-*psionic* form factors describe a different process, the form of the hadron current matrix element for the charmonia process is the same as that for the virtual photon one [9, 31]. Previous studies often neglected the polarization effects of hyperons [32–37]. However, Σ^+ polarization was recently observed and measured in the $e^+e^- \rightarrow J/\psi$, $\psi(3686) \rightarrow \Sigma^+\bar{\Sigma}^-$ processes by the BESIII collaboration [38, 39]. The results not only reveal a non-zero relative phase but also demonstrate that the phase changes sign at the mass of the $\psi(3686)$ resonance compared to the value measured at the J/ψ resonance. Subsequently, the polarization effects of Λ and Ξ^- were also observed and measured by the BESIII collaboration. The Λ polarization was observed in the $e^+e^- \rightarrow \Lambda\bar{\Lambda}$ process at the J/ψ , $\psi(3770)$, and off-resonance regions [29, 30, 40, 41]. Additionally, a non-zero polarization has been observed for Ξ^- in the $e^+e^- \rightarrow J/\psi$, $\psi(3686) \rightarrow \Xi^-\bar{\Xi}^+$ processes [42–44]. However, for Ξ^0 , completely different effects were observed in processes $e^+e^- \rightarrow J/\psi \rightarrow \Xi^0\bar{\Xi}^0$ [45] and $e^+e^- \rightarrow \psi(3686) \rightarrow \Xi^0\bar{\Xi}^0$ [46]. The data samples used in this analysis correspond to an integrated luminosity of 652.1 pb^{-1} , collected at the center-of-mass (CM) energies of $\sqrt{s} = 3.682, 3.683, 3.684, 3.685, 3.687, 3.691, \text{ and } 3.710 \text{ GeV}$ with the BESIII detector [47] in symmetric e^+e^- collisions provided by the BEPCII storage ring [48]. The above energy points around $\psi(3686)$ resonance, which are used to study the energy dependence of $\Delta\Phi$, are particularly intriguing, as the production occurs through a combination of one-photon exchange [49], mixing with the $\psi(3686)$ resonance [29], and resonance dominance [40, 41]. Since the energy range studied here includes both the virtual photon vector charmonium processes, $G_E^{\gamma/\Psi}$ and $G_M^{\gamma/\Psi}$ are used to represent the form factors in the following, and the methods used in the following apply to both processes.

2 BESIII detector and Monte Carlo simulation

The BESIII detector [47] records symmetric e^+e^- collisions provided by the BEPCII storage ring [48] in the CM energy ranging from 1.84 to 4.95 GeV, with a peak luminosity of $1 \times 10^{33} \text{ cm}^{-2} \text{ s}^{-1}$ achieved at $\sqrt{s} = 3.773 \text{ GeV}$. BESIII has collected large data samples in this energy region [50–52]. The cylindrical core of the BESIII detector covers 93% of the full solid angle and consists of a helium-based multilayer drift chamber (MDC), a plastic scintillator barrel and multigap resistive plate chamber end cap time-of-flight system (TOF), and a CsI(Tl) electromagnetic calorimeter (EMC), all enclosed in a superconducting solenoidal magnet providing a 1.0 T magnetic field. The solenoid is supported by an octagonal flux-return yoke with resistive plate counter muon identification modules interleaved with steel. The charged-particle momentum resolution at 1 GeV/ c is 0.5%, and the dE/dx resolution is 6% for electrons from Bhabha scattering. The EMC measures photon energies with a resolution of 2.5% (5%) at 1 GeV in the barrel (end cap) region. The time resolution in the TOF barrel region is 68 ps, while that in the end cap region is 60 ps [53–55].

To evaluate detection efficiencies and estimate backgrounds, simulated data samples are produced using GEANT4-based Monte Carlo (MC) software [56], which incorporates the geometric description of the BESIII detector [57] as well as the detector response. The simulation models the beam energy spread and initial-state radiation (ISR) effect in the e^+e^- annihilation process with KKMC [58]. The detection efficiency for the $e^+e^- \rightarrow \Sigma^+\bar{\Sigma}^-$ process is determined through MC simulations. For each of the 7 energy points ranging from 3.68 to 3.71 GeV, a sample of 100,000 events is simulated with a uniform phase space (PHSP) distribution. The $\Sigma^+(\bar{\Sigma}^-)$ baryon and its subsequent decays are simulated using EVTGEN [59, 60] with a PHSP model.

3 Event selection

A double-tag technique is employed in the event selection involving the decays of $\Sigma^+ \rightarrow p\pi^0$ and $\bar{\Sigma}^- \rightarrow \bar{p}\pi^0$ with the subsequent decay $\pi^0 \rightarrow \gamma\gamma$. Hence, in the final state, there are two charged particles, a proton and an anti-proton, along with four photons utilized for the reconstruction of two π^0 s. Consequently, suitable candidates must meet the following event selection criteria.

Charged tracks detected in the MDC are required to be within a polar angle (θ) range of $|\cos\theta| < 0.93$, where θ is defined with respect to the z -axis, which is the symmetry axis of the MDC. At least two oppositely charged tracks, which must be well reconstructed in the MDC with good helix fits, are required. There is no vertex requirement. Since (anti-)protons from $\Sigma^+(\bar{\Sigma}^-)$ decays can be distinguished from other charged particles by requiring the momentum to be greater than 0.5 GeV/ c , there is no additional particle identification (PID) requirement.

Showers deposited in the EMC are used to reconstruct π^0 s. The deposited energy of each shower must be more than 25 MeV in the barrel region ($|\cos\theta| < 0.80$) and more than 50 MeV in the end cap region ($0.86 < |\cos\theta| < 0.92$). To suppress electronic noise and

showers unrelated to the event, the difference between the EMC time and the event start time is required to be within [0, 700] ns. After selection, at least four photons are required.

To select the correct combination of proton, anti-proton, and $\pi^0\pi^0$ candidates, a six-constraint (6C) kinematic fit is applied to all $p\bar{p}\gamma\gamma\gamma\gamma$ combinations in each event. The 6C kinematic fit conserves energy and momentum while constraining the invariant mass of photon combinations to the known π^0 mass [61]. The $p\bar{p}\pi^0\pi^0$ combination with the smallest χ^2 is retained, and $\chi_{6C}^2 < 100$ is required to suppress the background. This requirement is determined by analyzing the figure-of-merit (FOM) $N_{\text{sig}}/\sqrt{N_{\text{sig}} + N_{\text{bkg}}}$, where N_{sig} and N_{bkg} represent the numbers of signal and background events, respectively, both based on MC simulation. To match p and \bar{p} with the correct π^0 , the $\Sigma^+\bar{\Sigma}^-$ pair with the minimum difference $\sqrt{(M_{p\pi^0} - m_{\Sigma^+})^2 + (M_{\bar{p}\pi^0} - m_{\bar{\Sigma}^-})^2}$ is selected for further analysis. Here, $M_{p\pi^0(\bar{p}\pi^0)}$ is the invariant mass of the $p\pi^0(\bar{p}\pi^0)$ combination, and $m_{\Sigma^+(\bar{\Sigma}^-)}$ is the known Σ^+ mass [61]. To eliminate the primary background originating from the $e^+e^- \rightarrow \pi^0\pi^0 J/\psi \rightarrow p\bar{p}\pi^0\pi^0$ process, the veto requirement $|M_{\pi^0\pi^0}^{\text{Recoil}} - m_{J/\psi}| > 15 \text{ MeV}/c^2$ is applied. Here, $M_{\pi^0\pi^0}^{\text{Recoil}}$ is the recoil mass of the $\pi^0\pi^0$ combination and $m_{J/\psi}$ is the mass of J/ψ [61]. This requirement is also determined by FOM optimization. Figure 1 shows the distribution of $M_{\bar{p}\pi^0}$ versus $M_{p\pi^0}$ of the accepted candidates summed over all energy points. The $M_{p\pi^0(\bar{p}\pi^0)}$ candidates are required to be within the range of $[m_{\Sigma^+} - 4\sigma, m_{\Sigma^+} + 3\sigma] \text{ MeV}/c^2$, denoted by S in figure 1, where the resolution σ is determined by a one-dimensional fit with the Crystal-Ball function [62]. Due to the energy leakage of the photon in the EMC, the signal shape is asymmetric.

After applying the event selection criteria to the data, the remaining background mainly comes from non- $\Sigma^+(\bar{\Sigma}^-)$ events, such as the non-resonant process $e^+e^- \rightarrow \pi^0\pi^0 p\bar{p}$. The number of background events is estimated using the sideband method, *i.e.* $\sum_{i=1}^4 B_i/4$ for the $M_{p\pi^0}$ and $M_{\bar{p}\pi^0}$ windows, where i runs over the four regions shown in figure 1, and the exact ranges are defined as $B_1: M_{p\pi^0} \in [1.119, 1.154] \text{ GeV}/c^2$ and $M_{\bar{p}\pi^0} \in [1.219, 1.254] \text{ GeV}/c^2$, $B_2: M_{p\pi^0} \in [1.219, 1.254] \text{ GeV}/c^2$ and $M_{\bar{p}\pi^0} \in [1.219, 1.254] \text{ GeV}/c^2$, $B_3: M_{p\pi^0} \in [1.119, 1.154] \text{ GeV}/c^2$ and $M_{\bar{p}\pi^0} \in [1.119, 1.154] \text{ GeV}/c^2$, $B_4: M_{p\pi^0} \in [1.219, 1.254] \text{ GeV}/c^2$ and $M_{\bar{p}\pi^0} \in [1.119, 1.154] \text{ GeV}/c^2$.

The signal yield combining all energy points is 898 ± 30 (stat.) events. The numbers of signal events for each energy point are listed in table 1. The number of background events estimated with the sideband method is 36 ± 3 (stat.), which is a background level of 3.85%.

4 Σ^+ polarization

The exclusive process $e^+e^- \rightarrow \gamma^*/\Psi \rightarrow \Sigma^+\bar{\Sigma}^- \rightarrow p\bar{p}\pi^0\pi^0$ can be fully described by the Σ^+ scattering angle, θ_{Σ^+} , in the CM system of the e^+e^- reaction and the p and \bar{p} directions, \hat{n}_1 and \hat{n}_2 , respectively, in the rest frames of their parent particles. Here γ^*/Ψ indicates that the process $e^+e^- \rightarrow \Sigma^+\bar{\Sigma}^-$ occurs via a pure EM process or a ψ resonance. The components of these vectors are expressed using a coordinate system $(x_{\Sigma^+}, y_{\Sigma^+}, z_{\Sigma^+})$ as shown in figure 2. A right-handed system for each hyperon decay is defined with the z axis along the Σ^+ momentum $\mathbf{p}_{\Sigma^+} = -\mathbf{p}_{\bar{\Sigma}^-} = \mathbf{p}$ in the CM system. The y axis is taken as the

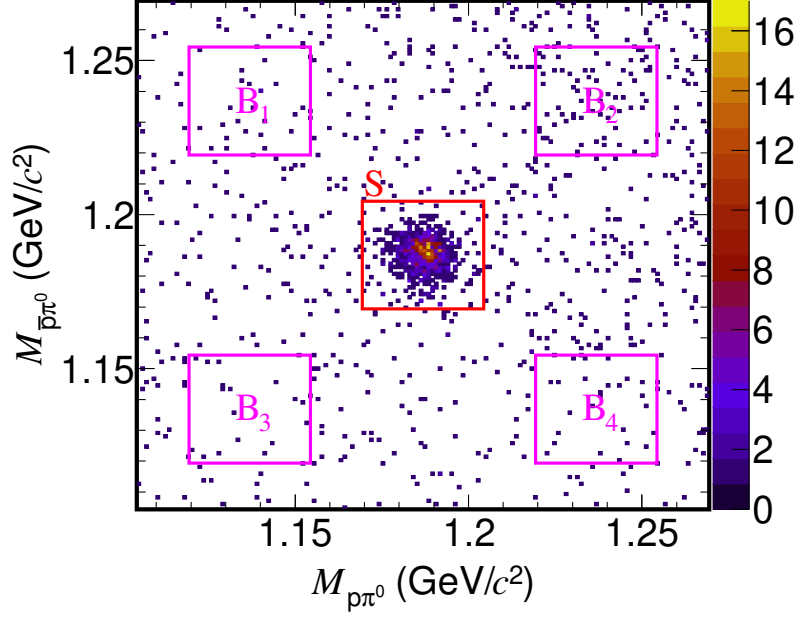


Figure 1. Two-dimensional distribution of $M_{\bar{p}\pi^0}$ versus $M_{p\pi^0}$ of the accepted candidates summed over all energy points, where the red square marked with S indicates the signal region, and the pink squares marked with B_i ($i = 1, 2, 3, 4$) show the selected background regions.

normal to the scattering plane, $\mathbf{k}_{e^-} \times \mathbf{p}_{\Sigma^+}$, where $\mathbf{k}_{e^-} = -\mathbf{k}_{e^+} = \mathbf{k}$ is the electron beam momentum in the CM system.

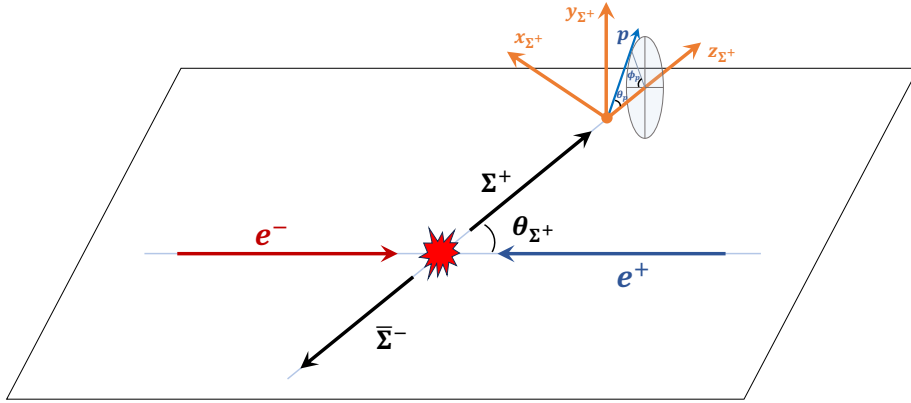


Figure 2. Definition of the coordinate system describing the $e^+e^- \rightarrow \gamma^*/\Psi \rightarrow \Sigma^+\bar{\Sigma}^- \rightarrow p\bar{p}\pi^0\pi^0$ reaction. The Σ^+ particle is emitted along the z_{Σ^+} axis direction, and the $\bar{\Sigma}^-$ in the opposite direction. The y_{Σ^+} axis is perpendicular to the plane of Σ^+ and e^- , and the x_{Σ^+} axis is defined by a right-handed coordinate system. The Σ^+ decay product, the proton, is measured in this coordinate system.

The joint decay angular distribution of the process $e^+e^- \rightarrow \gamma^*/\Psi \rightarrow \Sigma^+\bar{\Sigma}^- \rightarrow p\bar{p}\pi^0\pi^0$, involving spin-entangled $\Sigma^+\bar{\Sigma}^-$, is expressed as [9]

$$\begin{aligned} \mathcal{W}(\boldsymbol{\xi}; \boldsymbol{\Omega}) = & \mathcal{F}_0(\xi) + \eta\mathcal{F}_5(\xi) + \alpha_{\Sigma^+}\alpha_{\bar{\Sigma}^-} \\ & \times [\mathcal{F}_1(\xi) + \sqrt{1-\eta^2}\cos(\Delta\Phi)\mathcal{F}_2(\xi) + \eta\mathcal{F}_6(\xi)] \\ & + \sqrt{1-\eta^2}\sin(\Delta\Phi)[\alpha_{\Sigma^+}\mathcal{F}_3(\xi) + \alpha_{\bar{\Sigma}^-}\mathcal{F}_4(\xi)], \end{aligned} \quad (4.1)$$

where η is the angular distribution parameter, $\boldsymbol{\Omega} = (\eta, \Delta\Phi, \alpha_{\Sigma^+}, \alpha_{\bar{\Sigma}^-})$ represents the production and decay parameters, the kinematic variables $\boldsymbol{\xi} = (\theta_{\Sigma^+}, \hat{\mathbf{n}}_1, \hat{\mathbf{n}}_2)$ describe the production and subsequent decay, and $\alpha_{\Sigma^+}(\alpha_{\bar{\Sigma}^-})$ denotes the asymmetry parameter of the $\Sigma^+(\bar{\Sigma}^-) \rightarrow p\pi^0(\bar{p}\pi^0)$ decay. The angular functions $\mathcal{F}_i(\xi)$ ($i = 0, 1, \dots, 6$) are described in detail in ref. [9], and the five that are functions of θ_{Σ^+} are shown in eq. (4.2).

$$\begin{aligned} F_1 &= \sum_{i=1}^{N_k} (\sin^2\theta_{\Sigma^+} n_{1,x}^i n_{2,x}^i + \cos^2\theta_{\Sigma^+} n_{1,z}^i n_{2,z}^i), \\ F_2 &= \sum_{i=1}^{N_k} \sin\theta_{\Sigma^+} \cos\theta_{\Sigma^+} (n_{1,x}^i n_{2,z}^i + n_{1,z}^i n_{2,x}^i), \\ F_3 &= \sum_{i=1}^{N_k} \sin\theta_{\Sigma^+} \cos\theta_{\Sigma^+} n_{1,y}^i, \\ F_4 &= \sum_{i=1}^{N_k} \sin\theta_{\Sigma^+} \cos\theta_{\Sigma^+} n_{2,y}^i, \\ F_5 &= \sum_{i=1}^{N_k} (n_{1,z}^i n_{2,z}^i - \sin^2\theta_{\Sigma^+} n_{1,y}^i n_{2,y}^i), \end{aligned} \quad (4.2)$$

where, N_k is the number of events in the k^{th} $\cos\theta_{\Sigma^+}$ interval, $n_{1,j}$ ($n_{2,j}$) ($j = x, y, z$) represents the component of vector $\hat{\mathbf{n}}_1$ ($\hat{\mathbf{n}}_2$) in the coordinate system $(x_{\Sigma^+}, y_{\Sigma^+}, z_{\Sigma^+})$, and i is the index from 1 to N_k .

The modulus ratio of the form factors, R [29], can be described by the angular distribution parameter η .

$$R = \frac{|G_E^{\gamma/\Psi}|}{|G_M^{\gamma/\Psi}|} = \sqrt{\frac{\tau(1-\eta)}{1+\eta}}, \quad (4.3)$$

where $\tau = \frac{s}{4m_{\Sigma^+}^2}$ and s is the square of the CM energy. If the initial state is unpolarized, and the production process is either strong or electromagnetic and hence parity-conserving, then a non-zero polarization is only possible in the transverse direction y . The polarization is given by [9]

$$P_y = \frac{\sqrt{1-\eta^2} \sin\theta_{\Sigma^+} \cos\theta_{\Sigma^+}}{1+\eta \cos^2\theta_{\Sigma^+}} \sin(\Delta\Phi). \quad (4.4)$$

To determine η and $\Delta\Phi$, an unbinned maximum likelihood fit is performed, where the decay parameters α_{Σ^+} and $\alpha_{\bar{\Sigma}^-}$ are fixed to the values -0.994 and 0.994 , respectively,

obtained from the average in ref. [38], assuming CP conservation. In the fit, the likelihood function \mathcal{L} is constructed from the probability function, $\mathcal{P}(\boldsymbol{\xi}_i)$, for event i characterized by the measured angles $\boldsymbol{\xi}_i$

$$\mathcal{L} = \prod_{i=1}^N \mathcal{P}(\boldsymbol{\xi}_i, \boldsymbol{\Omega}) = \prod_{i=1}^N \mathcal{C} \mathcal{W}(\boldsymbol{\xi}_i, \boldsymbol{\Omega}) \epsilon(\boldsymbol{\xi}_i), \quad (4.5)$$

where N is the number of events in the signal region, and $\epsilon(\boldsymbol{\xi}_i)$ is the detection efficiency. For the ISR effect at the higher energy points 3.691 and 3.710 GeV, MC studies are performed where the input cross section for $e^+e^- \rightarrow \Sigma^+\bar{\Sigma}^-$ for calculating the ISR effect is taken from ref. [63]. The ISR effect at these two energy points brings absolute differences of 0.02 and 0.04 rad for η and $\Delta\Phi$, respectively, which are negligible. The normalization factor $\mathcal{C} = \frac{1}{N_{\text{MC}}} \sum_{j=1}^{N_{\text{MC}}} \mathcal{W}(\boldsymbol{\xi}^j, \boldsymbol{\Omega})$ is given by the sum of the corresponding angular distribution function \mathcal{W} using the accepted MC events, N_{MC} , and the difference in efficiency between data and MC simulations is taken into account as a systematic uncertainty, described later. The minimization of the function

$$\mathcal{S} = -\ln \mathcal{L}_{\text{data}} \quad (4.6)$$

is performed with RooFit [64]. Here, $\mathcal{L}_{\text{data}}$ is the likelihood function of events selected in the signal region.

Figure 3 shows the distributions of the five F_k ($k = 1, 2, \dots, 5$) moments [9] with respect to $\cos \theta_{\Sigma^+}$, divided into 10 intervals, and the weighted PHSP MC results corrected by the global fit. The numerical fit results and the weighted average values are summarized in table 1. Here, the weighted average is calculated by $\frac{1}{w} \sum_{i=1}^n w_i x_i$ [61], where n is the number of energy points, $w_i = 1/\sigma_i^2$, x_i and σ_i are the measured values and their uncertainties at each energy point, respectively, and $w = \sum_i w_i$. The relative phases of the form factors at each energy point are measured to be different from zero with significances of less than 3σ . The significance is estimated by comparing the likelihoods of the baseline fit and the one defined assuming no polarization [65]. The calculation of significance also accounts for the systematic uncertainties in the decay parameter, mass window, and background. After evaluating the significance following each systematic uncertainty, we select the smallest value as a conservative estimation. The significance of each energy point is also summarized in table 1.

Figure 4 shows the distribution of the moment given by

$$M(\cos \theta_{\Sigma^+}) = \frac{m}{N} \sum_{i=1}^{N_k} (n_{1,y}^i - n_{2,y}^i), \quad (4.7)$$

which is calculated for $m = 10$ intervals in $\cos \theta_{\Sigma^+}$. Here, N represents the total number of events in the data sample. According to ref. [40], $M(\cos \theta_{\Sigma^+})$ is related to the polarization by

$$M(\cos \theta_{\Sigma^+}) = \frac{\alpha_{\Sigma^+} - \alpha_{\Sigma^-}}{2} \frac{1 + \eta \cos^2 \theta_{\Sigma^+}}{3 + \eta} P_y(\theta_{\Sigma^+}) \quad (4.8)$$

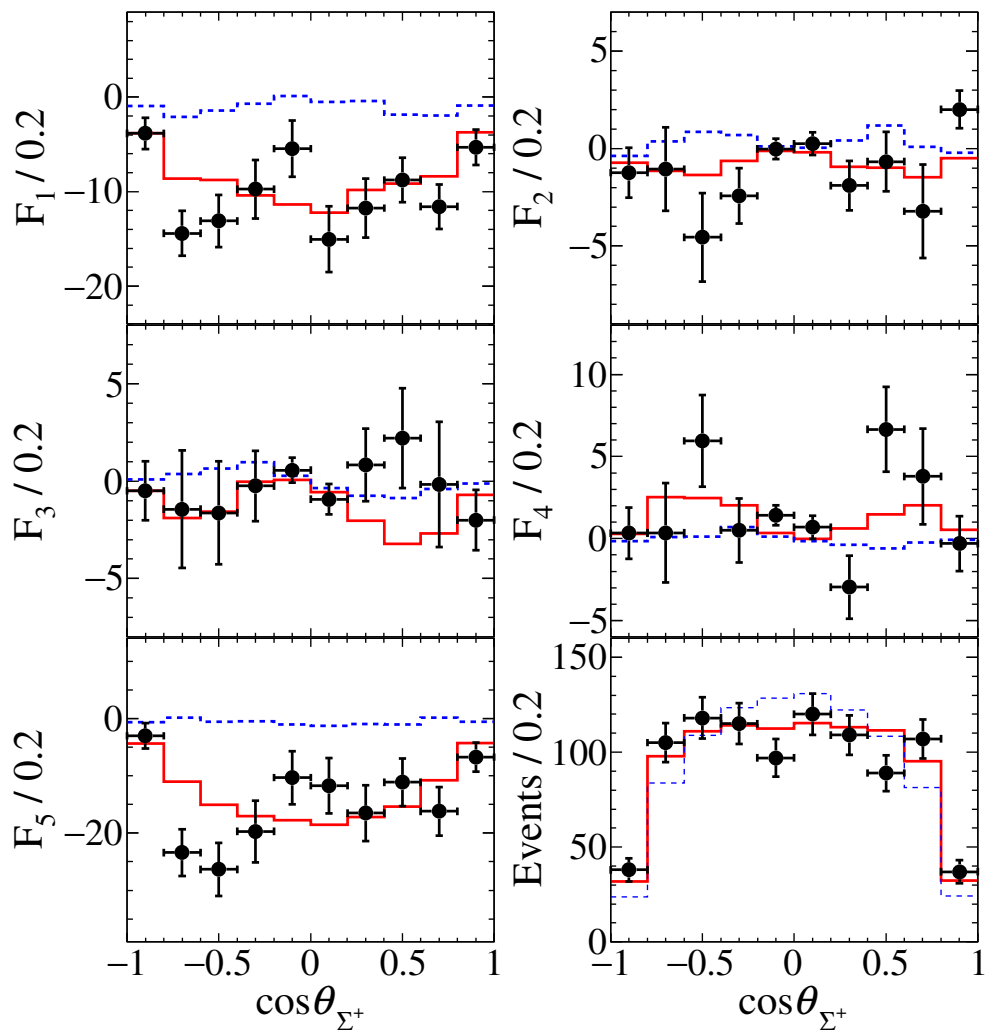


Figure 3. Distributions of F_k ($k = 1, 2, \dots, 5$) moments with respect to $\cos\theta_{\Sigma^+}$. The dots with error bars are data combined from all energy points, and the red solid lines are the weighted PHSP MC corrected by the results of global fit. The blue dashed lines represent the distributions of the simulated events evenly distributed in PHSP, without polarization.

Assuming CP conservation, we have $\alpha_{\Sigma^+} = -\alpha_{\bar{\Sigma}^-}$, and the expected angular dependence of $M(\cos\theta_{\Sigma^+})$ is proportional to $\sqrt{1 - \eta^2} \alpha_{\Sigma^+} \sin\Delta\Phi \cos\theta_{\Sigma^+} \sin\theta_{\Sigma^+} / (3 + \eta)$, which is consistent with the data in figure 4.

5 Systematic uncertainty

The systematic uncertainties on the measurement of the Σ^+ hyperon polarization arise due to the $\Sigma^+(\bar{\Sigma}^-)$ reconstruction, the requirements on the $p\pi^0(\bar{p}\pi^0)$ mass window, the background estimation, the fit method, and the decay parameters $\alpha_{\Sigma^+/\bar{\Sigma}^-}$.

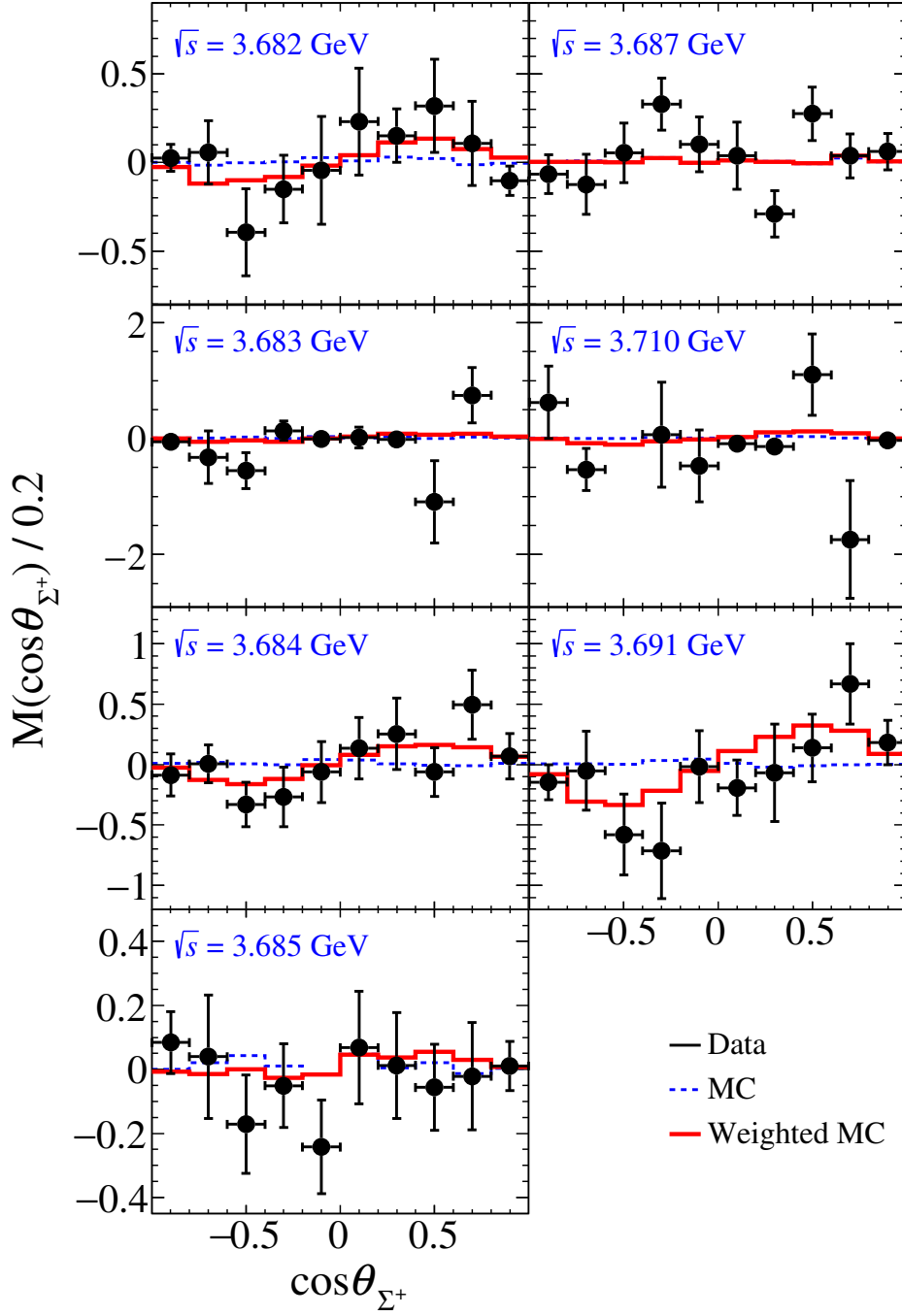


Figure 4. The moment $M(\cos\theta_{\Sigma^+})$ as a function of $\cos\theta_{\Sigma^+}$ for the $e^+e^- \rightarrow \Sigma^+\bar{\Sigma}^-$ reaction at different CM energies. Points with error bars are data, the red solid lines are the weighted PHSP MC corrected by the results of global fit, and the blue dashed lines represent the distributions without polarization from simulated events, evenly distributed in the PHSP.

Table 1. The number of observed events, N_{obs} , integrated luminosities, $\int \mathcal{L} dt$, measured parameters η , $\Delta\Phi$ and R for each energy point, the weighted average values, and the significance of the $\Delta\Phi$, S . The first uncertainty is statistical and the second one is systematic.

\sqrt{s} (GeV)	$\int \mathcal{L} dt$ (pb $^{-1}$)	N_{obs}	η	$\Delta\Phi$ (rad)	R	$S(\sigma)$
3.6820	404.0	$134.2^{+12.4}_{-11.8}$	$0.54 \pm 0.17 \pm 0.12$	$0.38 \pm 0.40 \pm 0.12$	$0.84 \pm 0.20 \pm 0.14$	0.4
3.6830	28.7	$27.2^{+6.0}_{-5.4}$	$0.96 \pm 0.13 \pm 0.12$	$2.35 \pm 1.66 \pm 0.12$	$0.22 \pm 0.37 \pm 0.34$	0.0
3.6840	28.7	$97.8^{+10.7}_{-10.1}$	$0.86 \pm 0.15 \pm 0.12$	$1.19 \pm 0.61 \pm 0.12$	$0.42 \pm 0.21 \pm 0.20$	1.9
3.6850	26.0	$256.2^{+16.8}_{-16.2}$	$0.76 \pm 0.10 \pm 0.12$	$0.16 \pm 0.32 \pm 0.12$	$0.57 \pm 0.15 \pm 0.16$	0.7
3.6870	25.1	$283.0^{+17.8}_{-16.8}$	$0.66 \pm 0.12 \pm 0.12$	$0.02 \pm 0.27 \pm 0.12$	$0.70 \pm 0.15 \pm 0.15$	0.4
3.6910	69.4	$77.5^{+9.8}_{-8.8}$	$0.16 \pm 0.23 \pm 0.12$	$1.29 \pm 0.54 \pm 0.12$	$1.31 \pm 0.30 \pm 0.16$	2.1
3.7100	70.3	$22.0^{+5.8}_{-4.7}$	$0.01 \pm 0.40 \pm 0.12$	$-2.64 \pm 0.60 \pm 0.12$	$1.55 \pm 0.62 \pm 0.19$	1.4
AVG.	-	-	$0.69 \pm 0.05 \pm 0.05$	$0.14 \pm 0.16 \pm 0.05$	$0.72 \pm 0.08 \pm 0.07$	-

5.1 $\Sigma^+(\bar{\Sigma}^-)$ reconstruction

The systematic uncertainty due to the $\Sigma^+(\bar{\Sigma}^-)$ reconstruction efficiency, incorporating the efficiencies of tracking, PID, kinematic fit and requirements of $M_{\pi^0\pi^0}^{\text{Recoil}}$ and π^0 reconstruction, is estimated using the control sample of $\psi(3686) \rightarrow \Sigma^+\bar{\Sigma}^-$ with the same method as described in refs. [66–68]. The efficiency difference is evaluated by comparing a full reconstruction sample that reconstructs both the baryon and anti-baryon sides, with two partial reconstruction samples that only reconstruct one side. The MC samples are then corrected with the efficiency difference, and the fit is repeated. The differences between the new and nominal values are taken as the systematic uncertainties.

5.2 Mass window

The uncertainty due to the requirements on the $p\pi^0(\bar{p}\pi^0)$ mass window is estimated with the same method as introduced in ref. [38]. The range of the $p\pi^0(\bar{p}\pi^0)$ mass window is increased or decreased by 1 MeV/ c^2 , and the maximum differences between the new and nominal values are taken as the systematic uncertainties.

5.3 Background

The systematic uncertainty associated with the background is determined by comparing the results obtained from the fits with and without considering the sideband background. The modified likelihood function is expressed as

$$\mathcal{S} = -\ln\mathcal{L}_{\text{data}} + \ln\mathcal{L}_{\text{bg}}, \quad (5.1)$$

where \mathcal{L}_{bg} is the likelihood function of background events determined in the sideband regions.

5.4 Fit method

To validate the reliability of the fit results, an input and output check is conducted using 500 pseudo-experiments. The helicity amplitude formula provided in ref. [9] is utilized. To ensure that the Gaussian function is fitted comprehensively, the input values of the polarization parameters are deliberately chosen to be far away from the fit boundary. In

order to ensure sufficient statistics, 6000 events are generated for each MC sample. In addition, to avoid the reconstruction effect, the MC samples used here have not been corrected by the detector. The differences between the input and output values obtained from the fits are negligible.

5.5 Decay parameter

The uncertainties from the decay parameters α_{Σ^+} for $\Sigma^+ \rightarrow p\pi^0$ and $\alpha_{\bar{\Sigma}^-}$ for $\bar{\Sigma}^- \rightarrow \bar{p}\pi^0$ are estimated by varying the value, obtained from averaging the results in ref. [38], by $\pm 1\sigma$. The largest differences in the result are taken as the systematic uncertainties.

5.6 Total systematic uncertainty

The systematic uncertainties on the polarization measurement are summarized in table 2. Assuming all sources are independent, the total systematic uncertainties are determined by adding these sources in quadrature.

Table 2. Absolute systematic uncertainties of the measured parameters.

Source	η	$\Delta\Phi$ (rad)
$\Sigma^+(\bar{\Sigma}^-)$ reconstruction	0.02	0.00
Mass window	0.01	0.02
Sideband background	0.11	0.11
Fit method	0.00	0.00
Decay parameter	0.05	0.03
Total	0.12	0.12

6 Summary

In summary, based on e^+e^- collision data corresponding to an integrated luminosity of 652.1 pb^{-1} collected with the BESIII detector at the BEPCII collider, we present an energy-dependent measurement of transverse polarization, relative phase and the modulus ratio of the form factors of Σ^+ hyperon in the $e^+e^- \rightarrow \Sigma^+\bar{\Sigma}^-$ reaction. For the first time, the phase of the Σ^+ hyperon electromagnetic form factors is explored in a higher range of four-momentum transfer above $q^2 > 13.5 \text{ GeV}^2$. No polarization is evident at each energy point. The comparison between this work and previous measurements [39, 69] is shown in figure 5. $\Delta\Phi$ is less than zero for J/ψ decay and $\sqrt{s} = 3.71 \text{ GeV}$, and greater than zero at other energy points, which implies that there may be at least one $\Delta\Phi = 0$ rad between these energy points. Such an evolution is important input for understanding its asymptotic behavior and the dynamics of baryons similar to the Λ hyperon [70]. These results are important to understand the production mechanism of the $\Sigma^+\bar{\Sigma}^-$ pairs at different energy points.

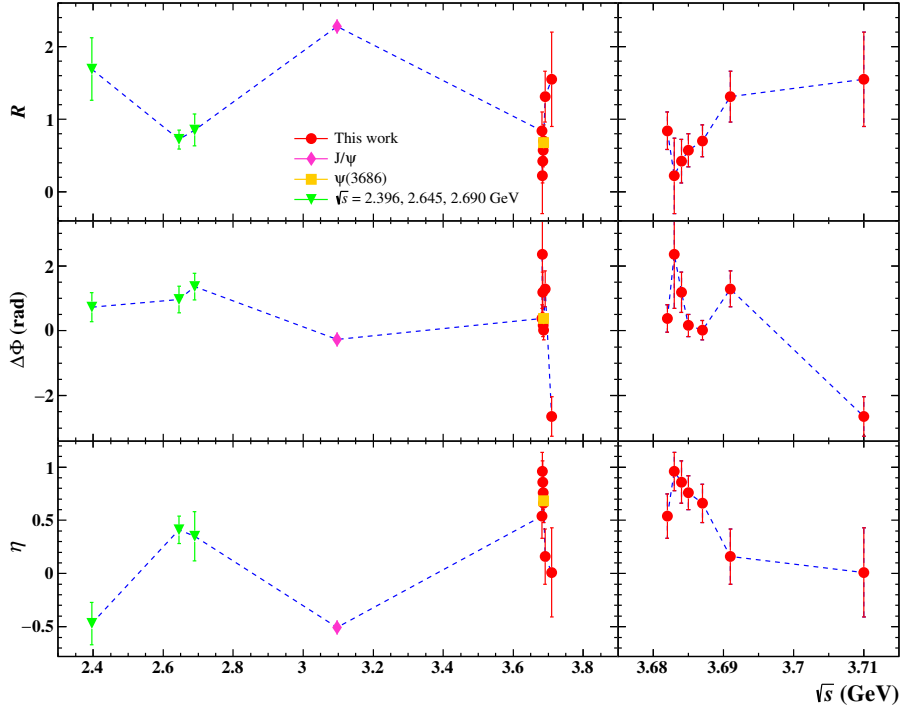


Figure 5. The comparisons of η , $\Delta\Phi$, and R as a function of CM energy between this work and the previous measurements [39, 69].

Acknowledgments

The BESIII Collaboration thanks the staff of BEPCII and the IHEP computing center for their strong support. This work is supported in part by National Key R&D Program of China under Contracts Nos. 2020YFA0406400, 2020YFA0406300, 2023YFA1606000; National Natural Science Foundation of China (NSFC) under Contracts Nos. 12075107, 12247101, 11635010, 11735014, 11835012, 11935015, 11935016, 11935018, 11961141012, 12025502, 12035009, 12035013, 12061131003, 12192260, 12192261, 12192262, 12192263, 12192264, 12192265, 12221005, 12225509, 12235017; the 111 Project under Grant No. B20063; the Chinese Academy of Sciences (CAS) Large-Scale Scientific Facility Program; the CAS Center for Excellence in Particle Physics (CCEPP); Joint Large-Scale Scientific Facility Funds of the NSFC and CAS under Contract No. U1832207; CAS Key Research Program of Frontier Sciences under Contracts Nos. QYZDJ-SSW-SLH003, QYZDJ-SSW-SLH040; 100 Talents Program of CAS; The Institute of Nuclear and Particle Physics (INPAC) and Shanghai Key Laboratory for Particle Physics and Cosmology; European Union’s Horizon 2020 research and innovation programme under Marie Skłodowska-Curie grant agreement under Contract No. 894790; German Research Foundation DFG under Contracts Nos. 455635585, Collaborative Research Center CRC 1044, FOR5327, GRK 2149; Istituto Nazionale di Fisica Nucleare, Italy; Ministry of Development of Turkey under Contract No. DPT2006K-120470; National Research Foundation of Korea under Contract No. NRF-2022R1A2C1092335; National Science and Technology fund of Mongolia;

National Science Research and Innovation Fund (NSRF) via the Program Management Unit for Human Resources & Institutional Development, Research and Innovation of Thailand under Contract No. B16F640076; Polish National Science Centre under Contract No. 2019/35/O/ST2/02907; The Swedish Research Council; U. S. Department of Energy under Contract No. DE-FG02-05ER41374

References

- [1] N. Cabibbo and R. Gatto, *Electron Positron Colliding Beam Experiments*, *Phys. Rev.* **124** (1961) 1577-1595 [INSPIRE].
- [2] C. F. Perdrisat, V. Punjabi and M. Vanderhaeghen, *Nucleon Electromagnetic Form Factors*, *Prog. Part. Nucl. Phys.* **59** (2007) 694 [arXiv:hep-ph/0612014] [INSPIRE].
- [3] M. A. Belushkin, H. W. Hammer and U. G. Meissner, *Dispersion analysis of the nucleon form-factors including meson continua*, *Phys. Rev. C* **75** (2007) 035202 [arXiv:hep-ph/0608337] [INSPIRE].
- [4] B. Yan, C. Chen and J. J. Xie, *Σ and Ξ electromagnetic form factors in the extended vector meson dominance model*, *Phys. Rev. D* **107** (2023) 076008 [arXiv:2301.00976] [INSPIRE].
- [5] G. S. Huang and R. B. Ferroli, *Probing the internal structure of baryons*, *Natl. Sci. Rev.* **8** (2021) nwab187 [arXiv:2111.08425] [INSPIRE].
- [6] BaBar Collaboration, *Study of $e^+e^- \rightarrow \Lambda\bar{\Lambda}$, $\Lambda\bar{\Sigma}^0$, $\Sigma^0\bar{\Sigma}^0$ using initial state radiation with BABAR*, *Phys. Rev. D* **76** (2007) 092006 [arXiv:0709.1988] [INSPIRE].
- [7] E. C. Titchmarsh, *The theory of functions*, Oxford university press (1939).
- [8] A. Z. Dubnickova, S. Dubnicka and M. P. Rekaló, *Investigation of the nucleon electromagnetic structure by polarization effects in $e^+e^- \rightarrow N\bar{N}$ processes*, *Nuovo Cim. A* **109** (1996) 241 [INSPIRE].
- [9] G. Fäldt and A. Kupsc, *Hadronic structure functions in the $e^+e^- \rightarrow \bar{\Lambda}\Lambda$ reaction*, *Phys. Lett. B* **772** (2017) 16 [arXiv:1702.07288] [INSPIRE].
- [10] X. Cao, J. P. Dai and H. Lenske, *Timelike nucleon electromagnetic form factors: All about interference of isospin amplitudes*, *Phys. Rev. D* **105** (2022) L071503 [arXiv:2109.15132] [INSPIRE].
- [11] J. P. Dai, X. Cao and H. Lenske, *Data driven isospin analysis of timelike octet baryons electromagnetic form factors and charmonium decay into baryon-anti-baryon*, *Phys. Lett. B* **846** (2023) 138192 [arXiv:2304.04913] [INSPIRE].
- [12] BESIII Collaboration, *Measurements of Σ^+ and Σ^- time-like electromagnetic form factors for center-of-mass energies from 2.3864 to 3.0200 GeV*, *Phys. Lett. B* **814** (2021) 136110 [arXiv:2009.01404] [INSPIRE].
- [13] Belle Collaboration, *Study of $e^+e^- \rightarrow \Sigma^0\bar{\Sigma}^0$ and $\Sigma^+\bar{\Sigma}^-$ by initial state radiation method at Belle*, *Phys. Rev. D* **107** (2023) 072008 [arXiv:2210.16761] [INSPIRE].
- [14] S. Dobbs, A. Tomaradze, T. Xiao, K. K. Seth and G. Bonvicini, *First measurements of timelike form factors of the hyperons, Λ^0 , Σ^0 , Σ^+ , Ξ^0 , Ξ^- , and Ω^- , and evidence of diquark correlations*, *Phys. Lett. B* **739** (2014) 90 [arXiv:1410.8356] [INSPIRE].
- [15] S. Dobbs, K. K. Seth, A. Tomaradze, T. Xiao and G. Bonvicini, *Hyperon Form Factors and Diquark Correlations*, *Phys. Rev. D* **96** (2017) 092004 [arXiv:1708.09377] [INSPIRE].

- [16] R. Jaffe, *Exotica*, *Phys. Rept.* **409** (2005) 1 [arXiv:hep-ph/0409065] [INSPIRE].
- [17] R. Jaffe, F. Wilczek, *Diquarks and exotic spectroscopy*, *Phys. Rev. Lett.* **91** (2003) 232003 [arXiv:hep-ph/0307341] [INSPIRE].
- [18] BESIII Collaboration, *Observation of a cross-section enhancement near mass threshold in $e^+e^- \rightarrow \Lambda\bar{\Lambda}$* , *Phys. Rev. D* **97** (2018) 032013 [arXiv:1709.10236] [INSPIRE].
- [19] BESIII Collaboration, *Measurement of cross section for $e^+e^- \rightarrow \Xi^-\bar{\Xi}^+$ near threshold at BESIII*, *Phys. Rev. D* **103** (2021) 012005 [arXiv:2010.08320] [INSPIRE].
- [20] BESIII Collaboration, *Measurement of cross section for $e^+e^- \rightarrow \Xi^0\bar{\Xi}^0$ near threshold*, *Phys. Lett. B* **820** (2021) 136557 [arXiv:2105.14657] [INSPIRE].
- [21] BESIII Collaboration, *Measurement of the $e^+e^- \rightarrow \Sigma^0\bar{\Sigma}^0$ cross sections at center-of-mass energies from 2.3864 to 3.0200 GeV*, *Phys. Lett. B* **831** (2022) 137187 [arXiv:2110.04510] [INSPIRE].
- [22] BESIII Collaboration, *Study of $e^+e^- \rightarrow \Omega^-\bar{\Omega}^+$ at center-of-mass energies from 3.49 to 3.67 GeV*, *Phys. Rev. D* **107** (2023) 052003 [arXiv:2212.03693] [INSPIRE].
- [23] X. Wang and G. Huang, *Electromagnetic Form Factor of Doubly-Strange Hyperon*, *Symmetry* **14** (2022) 65 [INSPIRE].
- [24] BESIII Collaboration, *Measurement of the cross section for $e^+e^- \rightarrow \Xi^-\bar{\Xi}^+$ and observation of an excited Ξ baryon*, *Phys. Rev. Lett.* **124** (2020) 032002 [arXiv:1910.04921] [INSPIRE].
- [25] BESIII Collaboration, *Measurement of the cross section for $e^+e^- \rightarrow \Lambda\bar{\Lambda}$ and evidence of the decay $\psi(3770) \rightarrow \Lambda\bar{\Lambda}$* , *Phys. Rev. D* **104** (2021) L091104 [arXiv:2108.02410] [INSPIRE].
- [26] BESIII Collaboration, *Measurement of the cross section of $e^+e^- \rightarrow \Xi^-\bar{\Xi}^+$ at center-of-mass energies between 3.510 and 4.843 GeV*, *JHEP* **11** (2023) 228 [arXiv:2309.04215] [INSPIRE].
- [27] BESIII Collaboration, *Measurement of Born cross section of $e^+e^- \rightarrow \Sigma^+\bar{\Sigma}^-$ at center-of-mass energies between 3.510 and 4.951 GeV*, *JHEP* **05** (2024) 022 [arXiv:2401.09468] [INSPIRE].
- [28] BESIII Collaboration, *Measurement of the cross sections of $e^+e^- \rightarrow K^-\bar{\Xi}^+\Lambda/\Sigma^0$ at center-of-mass energies between 3.510 and 4.914 GeV*, *JHEP* **07** (2024) 258 [arXiv:2406.18183] [INSPIRE].
- [29] BESIII Collaboration, *Measurement of Λ baryon polarization in $e^+e^- \rightarrow \Lambda\bar{\Lambda}$ at $\sqrt{s} = 3.773$ GeV*, *Phys. Rev. D* **105** (2022) L011101 [arXiv:2111.11742] [INSPIRE].
- [30] BESIII Collaboration, *Measurement of Λ transverse polarization in e^+e^- collisions at $\sqrt{s} = 3.68 - 3.71$ GeV*, *JHEP* **10** (2023) 081, [erratum: *JHEP* **12** (2023) 080] [arXiv:2303.00271] [INSPIRE].
- [31] G. Fäldt, *Polarization observables in the $e^+e^- \rightarrow \bar{\Lambda}\Lambda$ reaction*, *Eur. Phys. J. A* **52** (2016) 141 [arXiv:1602.02532] [INSPIRE].
- [32] BESIII Collaboration, *Measurements of baryon pair decays of χ_{cJ} mesons*, *Phys. Rev. D* **87** (2013) 032007 [arXiv:1211.2283] [INSPIRE].
- [33] BESIII Collaboration, *Study of ψ decays to the $\Xi^-\bar{\Xi}^+$ and $\Sigma(1385)^{\mp}\bar{\Sigma}(1385)^{\pm}$ final states*, *Phys. Rev. D* **93** (2016) 072003 [arXiv:1602.06754] [INSPIRE].
- [34] BESIII Collaboration, *Study of J/ψ and $\psi(3686) \rightarrow \Sigma(1385)^0\bar{\Sigma}(1385)^0$ and $\Xi^0\bar{\Xi}^0$* , *Phys. Lett. B* **770** (2017) 217 [arXiv:1612.08664] [INSPIRE].

- [35] BESIII Collaboration, *Observation of $\psi(3686) \rightarrow \Xi(1530)^-\bar{\Xi}(1530)^+$ and $\Xi(1530)^-\bar{\Xi}^+$* , *Phys. Rev. D* **100** (2019) 051101 [arXiv:1907.13041] [INSPIRE].
- [36] X. F. Wang, B. Li, Y. N. Gao and X. C. Lou, *Helicity amplitude analysis of J/ψ and $\psi(3686) \rightarrow \Xi(1530)\bar{\Xi}(1530)$* , *Nucl. Phys. B* **941** (2019) 861 [arXiv:1811.11352] [INSPIRE].
- [37] X. F. Wang, *Study of baryon pair production at BESIII*, *PoS CHARM2020* (2021) 026 [INSPIRE].
- [38] BESIII Collaboration, *Σ^+ and $\bar{\Sigma}^-$ polarization in the J/ψ and $\psi(3686)$ decays*, *Phys. Rev. Lett.* **125** (2020) 052004 [arXiv:2004.07701] [INSPIRE].
- [39] BESIII Collaboration, *Test of CP Symmetry in Hyperon to Neutron Decays*, *Phys. Rev. Lett.* **131** (2023) 191802 [arXiv:2304.146551] [INSPIRE].
- [40] BESIII Collaboration, *Precise Measurements of Decay Parameters and CP Asymmetry with Entangled $\Lambda - \bar{\Lambda}$ Pairs*, *Phys. Rev. Lett.* **129** (2022) 131801 [arXiv:2204.11058] [INSPIRE].
- [41] BESIII Collaboration, *Polarization and Entanglement in Baryon-Antibaryon Pair Production in Electron-Positron Annihilation*, *Nature Phys.* **15** (2019) 631 [arXiv:1808.08917] [INSPIRE].
- [42] BESIII Collaboration, *Probing CP symmetry and weak phases with entangled double-strange baryons*, *Nature* **606** (2022) 64 [arXiv:2105.11155] [INSPIRE].
- [43] BESIII Collaboration, *Observation of Ξ^- hyperon transverse polarization in $\psi(3686) \rightarrow \Xi^-\bar{\Xi}^+$* , *Phys. Rev. D* **106** (2022) L091101 [arXiv:2206.10900] [INSPIRE].
- [44] H. Liu, J. Zhang and X. Wang, *CP Asymmetry in the Ξ Hyperon Sector*, *Symmetry* **15** (2023) 214 [INSPIRE].
- [45] BESIII Collaboration, *Tests of CP symmetry in entangled Ξ^0 - $\bar{\Xi}^0$ pairs*, *Phys. Rev. D* **108** (2023) L031106 [arXiv:2305.09218] [INSPIRE].
- [46] BESIII Collaboration, *First simultaneous measurement of Ξ^0 and $\bar{\Xi}^0$ asymmetry parameters in $\psi(3686)$ decay*, *Phys. Rev. D* **108** (2023) L011101 [arXiv:2302.09767] [INSPIRE].
- [47] BESIII Collaboration, *Design and Construction of the BESIII Detector*, *Nucl. Instrum. Meth. A* **614** (2010) 345 [arXiv:0911.4960] [INSPIRE].
- [48] C. Yu et al., *BEPCII Performance and Beam Dynamics Studies on Luminosity*, *Proceedings, 7th International Particle Accelerator Conference (IPAC 2016)* May 8-13 2016 [INSPIRE].
- [49] BESIII Collaboration, *Complete Measurement of the Λ Electromagnetic Form Factors*, *Phys. Rev. Lett.* **123** (2019) 122003 [arXiv:1903.09421] [INSPIRE].
- [50] BESIII Collaboration, *Future Physics Programme of BESIII*, *Chin. Phys. C* **44** (2020) 040001 [arXiv:1912.05983] [INSPIRE].
- [51] J. Lu, Y. Xiao, and X. Ji, *Online monitoring of the center-of-mass energy from real data at BESIII*, *Radiat Detect Technol Methods* **4** (2020) 337.
- [52] J. W. Zhang, L. H. Wu, and S. S. Sun et al., *Suppression of top-up injection backgrounds with offline event filter in the BESIII experiment*, *Radiat. Detect. Technol. Methods* **6** (2022) 289 [INSPIRE].
- [53] X. Li et al., *Study of MRPC technology for BESIII endcap-TOF upgrade*, *Radiat. Detect. Technol. Methods* **1** (2017) 13.

- [54] Y. X. Guo *et al.*, *The study of time calibration for upgraded end cap TOF of BESIII*, *Radiat. Detect. Technol. Methods* **1** (2017) 15.
- [55] P. Cao *et al.*, *Design and construction of the new BESIII endcap Time-of-Flight system with MRPC Technology*, *Nucl. Instrum. Meth. A* **953** (2020) 163053 [INSPIRE].
- [56] GEANT4 Collaboration, *GEANT4—a simulation toolkit*, *Nucl. Instrum. Meth. A* **506** (2003) 250.
- [57] K. X. Huang, Z. J. Li, Z. Qian, J. Zhu, H. Y. Li, Y. M. Zhang, S. S. Sun and Z. Y. You, *Method for detector description transformation to Unity and application in BESIII*, *Nucl. Sci. Tech.* **33** (2022) 142 [arXiv:2206.10117] [INSPIRE].
- [58] S. Jadach, B. F. L. Ward and Z. Was, *Coherent exclusive exponentiation for precision Monte Carlo calculations*, *Phys. Rev. D* **63** (2001) 113009 [arXiv:hep-ph/0006359] [INSPIRE].
- [59] D. J. Lange, *The EvtGen particle decay simulation package*, *Nucl. Instrum. Meth. A* **462** (2001) 152.
- [60] R. G. Ping, *Event generators at BESIII*, *Chin. Phys. C* **32** (2008) 599.
- [61] Particle Data Group, *Review of Particle Physics*, *Phys. Rev. D* **110** (2024) 030001.
- [62] M. Oreglia, *A Study of the Reactions $\psi' \rightarrow \gamma\gamma\psi$* , *SLAC-R-0236* (1980) [INSPIRE].
- [63] KEDR Collaboration, *Final analysis of KEDR data on J/ψ and $\psi(2S)$ masses*, *Phys. Lett. B* **749** (2015) 50 [INSPIRE].
- [64] W. Verkerke and D. P. Kirkby, *The RooFit toolkit for data modeling*, eConf **C0303241** (2003) MOLT007 [arXiv:physics/0306116] [INSPIRE].
- [65] Y. S. Zhu, *On Statistical Significance of Signal*, *High Ener. Phys. Nucl. Phys.* **30** (2006) 331 [arXiv:0507145] [INSPIRE].
- [66] BESIII Collaboration, *Observation of $\psi(3686) \rightarrow \Xi(1530)^0 \bar{\Xi}(1530)^0$ and $\Xi(1530)^0 \bar{\Xi}^0$* , *Phys. Rev. D* **104** (2021) 092012 [arXiv:2109.06621] [INSPIRE].
- [67] BESIII Collaboration, *Study of the processes $\chi_{cJ} \rightarrow \Xi^- \bar{\Xi}^+$ and $\Xi^0 \bar{\Xi}^0$* , *JHEP* **06** (2022) 74 [arXiv:2202.08058] [INSPIRE].
- [68] BESIII Collaboration, *Partial wave analysis of $\psi(3686) \rightarrow \Lambda \bar{\Sigma}^0 \pi^0 + c.c.$* , [arXiv:2408.00495].
- [69] BESIII Collaboration, *Determination of the Σ^+ Timelike Electromagnetic Form Factors*, *Phys. Rev. Lett.* **132** (2024) 081904 [arXiv:2307.15894] [INSPIRE].
- [70] A. Mangoni, S. Pacetti and E. Tomasi-Gustafsson, *The first exploration of the physical Riemann surfaces of the ratio G_E^Λ/G_M^Λ* , *Phys. Rev. D* **104** (2021) 116016 [arXiv:2109.03759] [INSPIRE].

The BESIII collaboration

M. Ablikim¹, M. N. Achasov^{4,c}, P. Adlarson⁷⁵, O. Afedulidis³, X. C. Ai⁸⁰, R. Aliberti³⁵, A. Amoroso^{74A,74C}, Q. An^{71,58,a}, Y. Bai⁵⁷, O. Bakina³⁶, I. Balossino^{29A}, Y. Ban^{46,h}, H.-R. Bao⁶³, V. Batotzkaya^{1,44}, K. Begzsuren³², N. Berger³⁵, M. Berlowski⁴⁴, M. Bertani^{28A}, D. Bettoni^{29A}, F. Bianchi^{74A,74C}, E. Bianco^{74A,74C}, A. Bortone^{74A,74C}, I. Boyko³⁶, R. A. Briere⁵, A. Brueggemann⁶⁸, H. Cai⁷⁶, X. Cai^{1,58}, A. Calcaterra^{28A}, G. F. Cao^{1,63}, N. Cao^{1,63}, S. A. Cetin^{62A}, J. F. Chang^{1,58}, G. R. Che⁴³, G. Chelkov^{36,b}, C. Chen⁴³, C. H. Chen⁹, Chao Chen⁵⁵, G. Chen¹, H. S. Chen^{1,63}, H. Y. Chen²⁰, M. L. Chen^{1,58,63}, S. J. Chen⁴², S. L. Chen⁴⁵, S. M. Chen⁶¹, T. Chen^{1,63}, X. R. Chen^{31,63}, X. T. Chen^{1,63}, Y. B. Chen^{1,58}, Y. Q. Chen³⁴, Z. J. Chen^{25,i}, Z. Y. Chen^{1,63}, S. K. Choi^{10A}, G. Cibinetto^{29A}, F. Cossio^{74C}, J. J. Cui⁵⁰, H. L. Dai^{1,58}, J. P. Dai⁷⁸, A. Dbeyssi¹⁸, R. E. de Boer³, D. Dedovich³⁶, C. Q. Deng⁷², Z. Y. Deng¹, A. Denig³⁵, I. Denysenko³⁶, M. Destefanis^{74A,74C}, F. De Mori^{74A,74C}, B. Ding^{66,1}, X. X. Ding^{46,h}, Y. Ding⁴⁰, Y. Ding³⁴, J. Dong^{1,58}, L. Y. Dong^{1,63}, M. Y. Dong^{1,58,63}, X. Dong⁷⁶, M. C. Du¹, S. X. Du⁸⁰, Y. Y. Duan⁵⁵, Z. H. Duan⁴², P. Egorov^{36,b}, Y. H. Fan⁴⁵, J. Fang^{1,58}, J. Fang⁵⁹, S. S. Fang^{1,63}, W. X. Fang¹, Y. Fang¹, Y. Q. Fang^{1,58}, R. Farinelli^{29A}, L. Fava^{74B,74C}, F. Feldbauer³, G. Felici^{28A}, C. Q. Feng^{71,58}, J. H. Feng⁵⁹, Y. T. Feng^{71,58}, M. Fritsch³, C. D. Fu¹, J. L. Fu⁶³, Y. W. Fu^{1,63}, H. Gao⁶³, X. B. Gao⁴¹, Y. N. Gao^{46,h}, Yang Gao^{71,58}, S. Garbolino^{74C}, I. Garzia^{29A,29B}, L. Ge⁸⁰, P. T. Ge⁷⁶, Z. W. Ge⁴², C. Geng⁵⁹, E. M. Gersabeck⁶⁷, A. Gilman⁶⁹, K. Goetzen¹³, L. Gong⁴⁰, W. X. Gong^{1,58}, W. Gradl³⁵, S. Gramigna^{29A,29B}, M. Greco^{74A,74C}, M. H. Gu^{1,58}, Y. T. Gu¹⁵, C. Y. Guan^{1,63}, A. Q. Guo^{31,63}, L. B. Guo⁴¹, M. J. Guo⁵⁰, R. P. Guo⁴⁹, Y. P. Guo^{12,g}, A. Guskov^{36,b}, J. Gutierrez²⁷, K. L. Han⁶³, T. T. Han¹, F. Hanisch³, X. Q. Hao¹⁹, F. A. Harris⁶⁵, K. K. He⁵⁵, K. L. He^{1,63}, F. H. Heinsius³, C. H. Heinz³⁵, Y. K. Heng^{1,58,63}, C. Herold⁶⁰, T. Holtmann³, P. C. Hong³⁴, G. Y. Hou^{1,63}, X. T. Hou^{1,63}, Y. R. Hou⁶³, Z. L. Hou¹, B. Y. Hu⁵⁹, H. M. Hu^{1,63}, J. F. Hu^{56,j}, S. L. Hu^{12,g}, T. Hu^{1,58,63}, Y. Hu¹, G. S. Huang^{71,58}, K. X. Huang⁵⁹, L. Q. Huang^{31,63}, X. T. Huang⁵⁰, Y. P. Huang¹, Y. S. Huang⁵⁹, T. Hussain⁷³, F. Hölzken³, N. Hüskens³⁵, N. in der Wiesche⁶⁸, J. Jackson²⁷, S. Janchiv³², J. H. Jeong^{10A}, Q. Ji¹, Q. P. Ji¹⁹, W. Ji^{1,63}, X. B. Ji^{1,63}, X. L. Ji^{1,58}, Y. Y. Ji⁵⁰, X. Q. Jia⁵⁰, Z. K. Jia^{71,58}, D. Jiang^{1,63}, H. B. Jiang⁷⁶, P. C. Jiang^{46,h}, S. S. Jiang³⁹, T. J. Jiang¹⁶, X. S. Jiang^{1,58,63}, Y. Jiang⁶³, J. B. Jiao⁵⁰, J. K. Jiao³⁴, Z. Jiao²³, S. Jin⁴², Y. Jin⁶⁶, M. Q. Jing^{1,63}, X. M. Jing⁶³, T. Johansson⁷⁵, S. Kabana³³, N. Kalantar-Nayestanaki⁶⁴, X. L. Kang⁹, X. S. Kang⁴⁰, M. Kavatsyuk⁶⁴, B. C. Ke⁸⁰, V. Khachatryan²⁷, A. Khoukaz⁶⁸, R. Kiuchi¹, O. B. Kolcu^{62A}, B. Kopf³, M. Kuessner³, X. Kui^{1,63}, N. Kumar²⁶, A. Kupsc^{44,75}, W. Kühn³⁷, J. J. Lane⁶⁷, P. Larin¹⁸, L. Lavezzi^{74A,74C}, T. T. Lei^{71,58}, Z. H. Lei^{71,58}, M. Lellmann³⁵, T. Lenz³⁵, C. Li⁴³, C. Li⁴⁷, C. H. Li³⁹, Cheng Li^{71,58}, D. M. Li⁸⁰, F. Li^{1,58}, G. Li¹, H. B. Li^{1,63}, H. J. Li¹⁹, H. N. Li^{56,j}, Hui Li⁴³, J. R. Li⁶¹, J. S. Li⁵⁹, K. Li¹, L. J. Li^{1,63}, L. K. Li¹, Lei Li⁴⁸, M. H. Li⁴³, P. R. Li^{38,k,l}, Q. M. Li^{1,63}, Q. X. Li⁵⁰, R. Li^{17,31}, S. X. Li¹², T. Li⁵⁰, W. D. Li^{1,63}, W. G. Li^{1,a}, X. Li^{1,63}, X. H. Li^{71,58}, X. L. Li⁵⁰, X. Y. Li^{1,63}, X. Z. Li⁵⁹, Y. G. Li^{46,h}, Z. J. Li⁵⁹, Z. Y. Li⁷⁸, C. Liang⁴², H. Liang^{71,58}, H. Liang^{1,63}, Y. F. Liang⁵⁴, Y. T. Liang^{31,63}, G. R. Liao¹⁴, L. Z. Liao⁵⁰, Y. P. Liao^{1,63}, J. Libby²⁶, A. Limphirat⁶⁰, C. C. Lin⁵⁵, D. X. Lin^{31,63}, T. Lin¹, B. J. Liu¹, B. X. Liu⁷⁶, C. Liu³⁴, C. X. Liu¹, F. Liu¹, F. H. Liu⁵³, Feng Liu⁶, G. M. Liu^{56,j}, H. Liu^{38,k,l}, H. B. Liu¹⁵, H. H. Liu¹, H. M. Liu^{1,63}, Huihui Liu²¹, J. B. Liu^{71,58}, J. Y. Liu^{1,63}, K. Liu^{38,k,l}, K. Y. Liu⁴⁰, Ke Liu²², L. Liu^{71,58}, L. C. Liu⁴³, Lu Liu⁴³, M. H. Liu^{12,g}, P. L. Liu¹, Q. Liu⁶³, S. B. Liu^{71,58}, T. Liu^{12,g}, W. K. Liu⁴³, W. M. Liu^{71,58}, X. Liu^{38,k,l}, X. Liu³⁹, Y. Liu^{38,k,l}, Y. Liu⁸⁰, Y. B. Liu⁴³, Z. A. Liu^{1,58,63}, Z. D. Liu⁹, Z. Q. Liu⁵⁰, X. C. Lou^{1,58,63}, F. X. Lu⁵⁹,

H. J. Lu²³, J. G. Lu^{1,58}, X. L. Lu¹, Y. Lu⁷, Y. P. Lu^{1,58}, Z. H. Lu^{1,63}, C. L. Luo⁴¹, J. R. Luo⁵⁹,
 M. X. Luo⁷⁹, T. Luo^{12,g}, X. L. Luo^{1,58}, X. R. Lyu⁶³, Y. F. Lyu⁴³, F. C. Ma⁴⁰, H. Ma⁷⁸, H. L. Ma¹,
 J. L. Ma^{1,63}, L. L. Ma⁵⁰, M. M. Ma^{1,63}, Q. M. Ma¹, R. Q. Ma^{1,63}, T. Ma^{71,58}, X. T. Ma^{1,63},
 X. Y. Ma^{1,58}, Y. Ma^{46,h}, Y. M. Ma³¹, F. E. Maas¹⁸, M. Maggiora^{74A,74C}, S. Malde⁶⁹, Y. J. Mao^{46,h},
 Z. P. Mao¹, S. Marcello^{74A,74C}, Z. X. Meng⁶⁶, J. G. Messchendorp^{13,64}, G. Mezzadri^{29A}, H. Miao^{1,63},
 T. J. Min⁴², R. E. Mitchell²⁷, X. H. Mo^{1,58,63}, B. Moses²⁷, N. Yu. Muchnoi^{4,c}, J. Muskalla³⁵,
 Y. Nefedov³⁶, F. Nerling^{18,e}, L. S. Nie²⁰, I. B. Nikolaev^{4,c}, Z. Ning^{1,58}, S. Nisar^{11,m}, Q. L. Niu^{38,k,l},
 W. D. Niu⁵⁵, Y. Niu⁵⁰, S. L. Olsen⁶³, Q. Ouyang^{1,58,63}, S. Pacetti^{28B,28C}, X. Pan⁵⁵, Y. Pan⁵⁷,
 A. Pathak³⁴, P. Patteri^{28A}, Y. P. Pei^{71,58}, M. Pelizaeus³, H. P. Peng^{71,58}, Y. Y. Peng^{38,k,l},
 K. Peters^{13,e}, J. L. Ping⁴¹, R. G. Ping^{1,63}, S. Plura³⁵, V. Prasad³³, F. Z. Qi¹, H. Qi^{71,58}, H. R. Qi⁶¹,
 M. Qi⁴², T. Y. Qi^{12,g}, S. Qian^{1,58}, W. B. Qian⁶³, C. F. Qiao⁶³, X. K. Qiao⁸⁰, J. J. Qin⁷², L. Q. Qin¹⁴,
 L. Y. Qin^{71,58}, X. P. Qin^{12,g}, X. S. Qin⁵⁰, Z. H. Qin^{1,58}, J. F. Qiu¹, Z. H. Qu⁷², C. F. Redmer³⁵,
 K. J. Ren³⁹, A. Rivetti^{74C}, M. Rolo^{74C}, G. Rong^{1,63}, Ch. Rosner¹⁸, S. N. Ruan⁴³, N. Salone⁴⁴,
 A. Sarantsev^{36,d}, Y. Schelhaas³⁵, K. Schoenning⁷⁵, M. Scodreggio^{29A}, K. Y. Shan^{12,g}, W. Shan²⁴,
 X. Y. Shan^{71,58}, Z. J. Shang^{38,k,l}, J. F. Shangguan¹⁶, L. G. Shao^{1,63}, M. Shao^{71,58}, C. P. Shen^{12,g},
 H. F. Shen^{1,8}, W. H. Shen⁶³, X. Y. Shen^{1,63}, B. A. Shi⁶³, H. Shi^{71,58}, H. C. Shi^{71,58}, J. L. Shi^{12,g},
 J. Y. Shi¹, Q. Q. Shi⁵⁵, S. Y. Shi⁷², X. Shi^{1,58}, J. J. Song¹⁹, T. Z. Song⁵⁹, W. M. Song^{34,1}, Y.
 J. Song^{12,g}, Y. X. Song^{46,h,n}, S. Sosio^{74A,74C}, S. Spataro^{74A,74C}, F. Stieler³⁵, Y. J. Su⁶³, G. B. Sun⁷⁶,
 G. X. Sun¹, H. Sun⁶³, H. K. Sun¹, J. F. Sun¹⁹, K. Sun⁶¹, L. Sun⁷⁶, S. S. Sun^{1,63}, T. Sun^{51,f},
 W. Y. Sun³⁴, Y. Sun⁹, Y. J. Sun^{71,58}, Y. Z. Sun¹, Z. Q. Sun^{1,63}, Z. T. Sun⁵⁰, C. J. Tang⁵⁴,
 G. Y. Tang¹, J. Tang⁵⁹, M. Tang^{71,58}, Y. A. Tang⁷⁶, L. Y. Tao⁷², Q. T. Tao^{25,i}, M. Tat⁶⁹,
 J. X. Teng^{71,58}, V. Thoren⁷⁵, W. H. Tian⁵⁹, Y. Tian^{31,63}, Z. F. Tian⁷⁶, I. Uman^{62B}, Y. Wan⁵⁵,
 S. J. Wang⁵⁰, B. Wang¹, B. L. Wang⁶³, Bo Wang^{71,58}, D. Y. Wang^{46,h}, F. Wang⁷², H. J. Wang^{38,k,l},
 J. J. Wang⁷⁶, J. P. Wang⁵⁰, K. Wang^{1,58}, L. L. Wang¹, M. Wang⁵⁰, N. Y. Wang⁶³, S. Wang^{12,g},
 S. Wang^{38,k,l}, T. Wang^{12,g}, T. J. Wang⁴³, W. Wang⁵⁹, W. Wang⁷², W. P. Wang^{35,71,o}, X. Wang^{46,h},
 X. F. Wang^{38,k,l}, X. J. Wang³⁹, X. L. Wang^{12,g}, X. N. Wang¹, Y. Wang⁶¹, Y. D. Wang⁴⁵, Y. F. Wang^{1,58,63},
 Y. L. Wang¹⁹, Y. N. Wang⁴⁵, Y. Q. Wang¹, Yaqian Wang¹⁷, Yi Wang⁶¹, Z. Wang^{1,58}, Z. L. Wang⁷²,
 Z. Y. Wang^{1,63}, Ziyi Wang⁶³, D. H. Wei¹⁴, F. Weidner⁶⁸, S. P. Wen¹, Y. R. Wen³⁹, U. Wiedner³,
 G. Wilkinson⁶⁹, M. Wolke⁷⁵, L. Wollenberg³, C. Wu³⁹, J. F. Wu^{1,8}, L. H. Wu¹, L. J. Wu^{1,63},
 X. Wu^{12,g}, X. H. Wu³⁴, Y. Wu^{71,58}, Y. H. Wu⁵⁵, Y. J. Wu³¹, Z. Wu^{1,58}, L. Xia^{71,58}, X. M. Xian³⁹,
 B. H. Xiang^{1,63}, T. Xiang^{46,h}, D. Xiao^{38,k,l}, G. Y. Xiao⁴², S. Y. Xiao¹, Y. L. Xiao^{12,g}, Z. J. Xiao⁴¹,
 C. Xie⁴², X. H. Xie^{46,h}, Y. Xie⁵⁰, Y. G. Xie^{1,58}, Y. H. Xie⁶, Z. P. Xie^{71,58}, T. Y. Xing^{1,63},
 C. F. Xu^{1,63}, C. J. Xu⁵⁹, G. F. Xu¹, H. Y. Xu^{66,2,p}, M. Xu^{71,58}, Q. J. Xu¹⁶, Q. N. Xu³⁰,
 W. Xu¹, W. L. Xu⁶⁶, X. P. Xu⁵⁵, Y. C. Xu⁷⁷, Z. P. Xu⁴², Z. S. Xu⁶³, F. Yan^{12,g}, L. Yan^{12,g},
 W. B. Yan^{71,58}, W. C. Yan⁸⁰, X. Q. Yan¹, H. J. Yang^{51,f}, H. L. Yang³⁴, H. X. Yang¹, T. Yang¹,
 Y. Yang^{12,g}, Y. F. Yang^{1,63}, Y. F. Yang⁴³, Y. X. Yang^{1,63}, Z. W. Yang^{38,k,l}, Z. P. Yao⁵⁰, M. Ye^{1,58},
 M. H. Ye⁸, J. H. Yin¹, Z. Y. You⁵⁹, B. X. Yu^{1,58,63}, C. X. Yu⁴³, G. Yu^{1,63}, J. S. Yu^{25,i}, T. Yu⁷²,
 X. D. Yu^{46,h}, Y. C. Yu⁸⁰, C. Z. Yuan^{1,63}, J. Yuan³⁴, J. Yuan⁴⁵, L. Yuan², S. C. Yuan^{1,63},
 Y. Yuan^{1,63}, Z. Y. Yuan⁵⁹, C. X. Yue³⁹, A. A. Zafar⁷³, F. R. Zeng⁵⁰, S. H. Zeng⁷², X. Zeng^{12,g},
 Y. Zeng^{25,i}, Y. J. Zeng^{1,63}, Y. J. Zeng⁵⁹, X. Y. Zhai³⁴, Y. C. Zhai⁵⁰, Y. H. Zhan⁵⁹, A. Q. Zhang^{1,63},
 B. L. Zhang^{1,63}, B. X. Zhang¹, D. H. Zhang⁴³, G. Y. Zhang¹⁹, H. Zhang⁸⁰, H. Zhang^{71,58}, H. C. Zhang^{1,58,63},
 H. H. Zhang³⁴, H. H. Zhang⁵⁹, H. Q. Zhang^{1,58,63}, H. R. Zhang^{71,58}, H. Y. Zhang^{1,58}, J. Zhang⁸⁰,
 J. Zhang⁵⁹, J. J. Zhang⁵², J. L. Zhang²⁰, J. Q. Zhang⁴¹, J. S. Zhang^{12,g}, J. W. Zhang^{1,58,63},

J. X. Zhang^{38,k,l}, J. Y. Zhang¹, J. Z. Zhang^{1,63}, Jianyu Zhang⁶³, L. M. Zhang⁶¹, Lei Zhang⁴², P. Zhang^{1,63}, Q. Y. Zhang³⁴, R. Y. Zhang^{38,k,l}, S. H. Zhang^{1,63}, Shulei Zhang^{25,i}, X. D. Zhang⁴⁵, X. M. Zhang¹, X. Y. Zhang⁵⁰, Y. Zhang⁷², Y. Zhang¹, Y. T. Zhang⁸⁰, Y. H. Zhang^{1,58}, Y. M. Zhang³⁹, Yan Zhang^{71,58}, Z. D. Zhang¹, Z. H. Zhang¹, Z. L. Zhang³⁴, Z. Y. Zhang⁷⁶, Z. Y. Zhang⁴³, Z. Z. Zhang⁴⁵, G. Zhao¹, J. Y. Zhao^{1,63}, J. Z. Zhao^{1,58}, L. Zhao¹, Lei Zhao^{71,58}, M. G. Zhao⁴³, N. Zhao⁷⁸, R. P. Zhao⁶³, S. J. Zhao⁸⁰, Y. B. Zhao^{1,58}, Y. X. Zhao^{31,63}, Z. G. Zhao^{71,58}, A. Zhemchugov^{36,b}, B. Zheng⁷², B. M. Zheng³⁴, J. P. Zheng^{1,58}, W. J. Zheng^{1,63}, Y. H. Zheng⁶³, B. Zhong⁴¹, X. Zhong⁵⁹, H. Zhou⁵⁰, J. Y. Zhou³⁴, L. P. Zhou^{1,63}, S. Zhou⁶, X. Zhou⁷⁶, X. K. Zhou⁶, X. R. Zhou^{71,58}, X. Y. Zhou³⁹, Y. Z. Zhou^{12,g}, J. Zhu⁴³, K. Zhu¹, K. J. Zhu^{1,58,63}, K. S. Zhu^{12,g}, L. Zhu³⁴, L. X. Zhu⁶³, S. H. Zhu⁷⁰, S. Q. Zhu⁴², T. J. Zhu^{12,g}, W. D. Zhu⁴¹, Y. C. Zhu^{71,58}, Z. A. Zhu^{1,63}, J. H. Zou¹, J. Zu^{71,58}

¹ *Institute of High Energy Physics, Beijing 100049, People's Republic of China*

² *Beihang University, Beijing 100191, People's Republic of China*

³ *Bochum Ruhr-University, D-44780 Bochum, Germany*

⁴ *Budker Institute of Nuclear Physics SB RAS (BINP), Novosibirsk 630090, Russia*

⁵ *Carnegie Mellon University, Pittsburgh, Pennsylvania 15213, USA*

⁶ *Central China Normal University, Wuhan 430079, People's Republic of China*

⁷ *Central South University, Changsha 410083, People's Republic of China*

⁸ *China Center of Advanced Science and Technology, Beijing 100190, People's Republic of China*

⁹ *China University of Geosciences, Wuhan 430074, People's Republic of China*

¹⁰ *Chung-Ang University, Seoul, 06974, Republic of Korea*

¹¹ *COMSATS University Islamabad, Lahore Campus, Defence Road, Off Raiwind Road, 54000 Lahore, Pakistan*

¹² *Fudan University, Shanghai 200433, People's Republic of China*

¹³ *GSI Helmholtzcentre for Heavy Ion Research GmbH, D-64291 Darmstadt, Germany*

¹⁴ *Guangxi Normal University, Guilin 541004, People's Republic of China*

¹⁵ *Guangxi University, Nanning 530004, People's Republic of China*

¹⁶ *Hangzhou Normal University, Hangzhou 310036, People's Republic of China*

¹⁷ *Hebei University, Baoding 071002, People's Republic of China*

¹⁸ *Helmholtz Institute Mainz, Staudinger Weg 18, D-55099 Mainz, Germany*

¹⁹ *Henan Normal University, Xinxiang 453007, People's Republic of China*

²⁰ *Henan University, Kaifeng 475004, People's Republic of China*

²¹ *Henan University of Science and Technology, Luoyang 471003, People's Republic of China*

²² *Henan University of Technology, Zhengzhou 450001, People's Republic of China*

²³ *Huangshan College, Huangshan 245000, People's Republic of China*

²⁴ *Hunan Normal University, Changsha 410081, People's Republic of China*

²⁵ *Hunan University, Changsha 410082, People's Republic of China*

²⁶ *Indian Institute of Technology Madras, Chennai 600036, India*

²⁷ *Indiana University, Bloomington, Indiana 47405, USA*

²⁸ *INFN Laboratori Nazionali di Frascati, (A)INFN Laboratori Nazionali di Frascati, I-00044, Frascati, Italy; (B)INFN Sezione di Perugia, I-06100, Perugia, Italy; (C)University of Perugia, I-06100, Perugia, Italy*

²⁹ *INFN Sezione di Ferrara, (A)INFN Sezione di Ferrara, I-44122, Ferrara, Italy; (B)University*

- of Ferrara, I-44122, Ferrara, Italy
- ³⁰ Inner Mongolia University, Hohhot 010021, People's Republic of China
- ³¹ Institute of Modern Physics, Lanzhou 730000, People's Republic of China
- ³² Institute of Physics and Technology, Peace Avenue 54B, Ulaanbaatar 13330, Mongolia
- ³³ Instituto de Alta Investigación, Universidad de Tarapacá, Casilla 7D, Arica 1000000, Chile
- ³⁴ Jilin University, Changchun 130012, People's Republic of China
- ³⁵ Johannes Gutenberg University of Mainz, Johann-Joachim-Becher-Weg 45, D-55099 Mainz, Germany
- ³⁶ Joint Institute for Nuclear Research, 141980 Dubna, Moscow region, Russia
- ³⁷ Justus-Liebig-Universität Giessen, II. Physikalisches Institut, Heinrich-Buff-Ring 16, D-35392 Giessen, Germany
- ³⁸ Lanzhou University, Lanzhou 730000, People's Republic of China
- ³⁹ Liaoning Normal University, Dalian 116029, People's Republic of China
- ⁴⁰ Liaoning University, Shenyang 110036, People's Republic of China
- ⁴¹ Nanjing Normal University, Nanjing 210023, People's Republic of China
- ⁴² Nanjing University, Nanjing 210093, People's Republic of China
- ⁴³ Nankai University, Tianjin 300071, People's Republic of China
- ⁴⁴ National Centre for Nuclear Research, Warsaw 02-093, Poland
- ⁴⁵ North China Electric Power University, Beijing 102206, People's Republic of China
- ⁴⁶ Peking University, Beijing 100871, People's Republic of China
- ⁴⁷ Qufu Normal University, Qufu 273165, People's Republic of China
- ⁴⁸ Renmin University of China, Beijing 100872, People's Republic of China
- ⁴⁹ Shandong Normal University, Jinan 250014, People's Republic of China
- ⁵⁰ Shandong University, Jinan 250100, People's Republic of China
- ⁵¹ Shanghai Jiao Tong University, Shanghai 200240, People's Republic of China
- ⁵² Shanxi Normal University, Linfen 041004, People's Republic of China
- ⁵³ Shanxi University, Taiyuan 030006, People's Republic of China
- ⁵⁴ Sichuan University, Chengdu 610064, People's Republic of China
- ⁵⁵ Soochow University, Suzhou 215006, People's Republic of China
- ⁵⁶ South China Normal University, Guangzhou 510006, People's Republic of China
- ⁵⁷ Southeast University, Nanjing 211100, People's Republic of China
- ⁵⁸ State Key Laboratory of Particle Detection and Electronics, Beijing 100049, Hefei 230026, People's Republic of China
- ⁵⁹ Sun Yat-Sen University, Guangzhou 510275, People's Republic of China
- ⁶⁰ Suranaree University of Technology, University Avenue 111, Nakhon Ratchasima 30000, Thailand
- ⁶¹ Tsinghua University, Beijing 100084, People's Republic of China
- ⁶² Turkish Accelerator Center Particle Factory Group, (A)Istinye University, 34010, Istanbul, Turkey; (B)Near East University, Nicosia, North Cyprus, 99138, Mersin 10, Turkey
- ⁶³ University of Chinese Academy of Sciences, Beijing 100049, People's Republic of China
- ⁶⁴ University of Groningen, NL-9747 AA Groningen, The Netherlands
- ⁶⁵ University of Hawaii, Honolulu, Hawaii 96822, USA
- ⁶⁶ University of Jinan, Jinan 250022, People's Republic of China

- ⁶⁷ *University of Manchester, Oxford Road, Manchester, M13 9PL, United Kingdom*
- ⁶⁸ *University of Muenster, Wilhelm-Klemm-Strasse 9, 48149 Muenster, Germany*
- ⁶⁹ *University of Oxford, Keble Road, Oxford OX13RH, United Kingdom*
- ⁷⁰ *University of Science and Technology Liaoning, Anshan 114051, People's Republic of China*
- ⁷¹ *University of Science and Technology of China, Hefei 230026, People's Republic of China*
- ⁷² *University of South China, Hengyang 421001, People's Republic of China*
- ⁷³ *University of the Punjab, Lahore-54590, Pakistan*
- ⁷⁴ *University of Turin and INFN, (A)University of Turin, I-10125, Turin, Italy; (B)University of Eastern Piedmont, I-15121, Alessandria, Italy; (C)INFN, I-10125, Turin, Italy*
- ⁷⁵ *Uppsala University, Box 516, SE-75120 Uppsala, Sweden*
- ⁷⁶ *Wuhan University, Wuhan 430072, People's Republic of China*
- ⁷⁷ *Yantai University, Yantai 264005, People's Republic of China*
- ⁷⁸ *Yunnan University, Kunming 650500, People's Republic of China*
- ⁷⁹ *Zhejiang University, Hangzhou 310027, People's Republic of China*
- ⁸⁰ *Zhengzhou University, Zhengzhou 450001, People's Republic of China*

^a *Deceased*

^b *Also at the Moscow Institute of Physics and Technology, Moscow 141700, Russia*

^c *Also at the Novosibirsk State University, Novosibirsk, 630090, Russia*

^d *Also at the NRC "Kurchatov Institute", PNPI, 188300, Gatchina, Russia*

^e *Also at Goethe University Frankfurt, 60323 Frankfurt am Main, Germany*

^f *Also at Key Laboratory for Particle Physics, Astrophysics and Cosmology, Ministry of Education; Shanghai Key Laboratory for Particle Physics and Cosmology; Institute of Nuclear and Particle Physics, Shanghai 200240, People's Republic of China*

^g *Also at Key Laboratory of Nuclear Physics and Ion-beam Application (MOE) and Institute of Modern Physics, Fudan University, Shanghai 200443, People's Republic of China*

^h *Also at State Key Laboratory of Nuclear Physics and Technology, Peking University, Beijing 100871, People's Republic of China*

ⁱ *Also at School of Physics and Electronics, Hunan University, Changsha 410082, China*

^j *Also at Guangdong Provincial Key Laboratory of Nuclear Science, Institute of Quantum Matter, South China Normal University, Guangzhou 510006, China*

^k *Also at MOE Frontiers Science Center for Rare Isotopes, Lanzhou University, Lanzhou 730000, People's Republic of China*

^l *Also at Lanzhou Center for Theoretical Physics, Key Laboratory of Theoretical Physics of Gansu Province, and Key Laboratory for Quantum Theory and Applications of MoE, Lanzhou University, Lanzhou 730000, People's Republic of China*

^m *Also at the Department of Mathematical Sciences, IBA, Karachi 75270, Pakistan*

ⁿ *Also at Ecole Polytechnique Federale de Lausanne (EPFL), CH-1015 Lausanne, Switzerland*

^o *Also at Helmholtz Institute Mainz, Staudinger Weg 18, D-55099 Mainz, Germany*

^p *Also at School of Physics, Beihang University, Beijing 100191, China*